


Background Measurements and Simulations of the ComPair Balloon Flight

Zachary Metzler^{1,2,3*} , Nicholas Kirschner^{2,4}, Lucas Smith^{1,2,3}, Nicholas Cannady², Makoto Sasaki^{1,2,3}, Daniel Shy⁵, Regina Caputo², Carolyn Kierans², Aleksey Bolotnikov⁶, Thomas J. Caligiure⁷, Gabriella A. Carini⁶, A. Wilder Crosier⁷, Jack Fried⁶, Priyarshini Ghosh^{2,3,8}, Sean Griffin⁹, J. Eric Grove⁵, Elizabeth Hays², Sven Herrmann⁶, Emily Kong¹⁰, Iker Liceaga-Indart², Julie McEnery², John Mitchell², A. A. Moiseev^{1,2,3}, Lucas Parker¹¹, Jeremy Perkins², Bernard Philips⁵, Adam J. Schoenwald², Clio Sleator⁵, D. J. Thompson², Janeth Valverde^{2,3,8}, Sambid Wasti^{2,3,12}, Richard Woolf⁵, Eric Wulf⁵, and Anna Zajczyk^{2,3,8}

¹ University of Maryland, College Park

² NASA Goddard Space Flight Center

³ Center for Research and Exploration in Space Science & Technology II

⁴ George Washington University

⁵ U.S. Naval Research Laboratory

⁶ Brookhaven National Laboratory

⁷ Naval Research Enterprise Internship Program, resident at U.S. Naval Research Laboratory

⁸ University of Maryland, Baltimore County

⁹ Wisconsin IceCube Particle Astrophysics Center

¹⁰ Technology Service Corporation

¹¹ Los Alamos National Laboratory

¹² Catholic University of America

* Correspondence: zmetzler@umd.edu

Received:

Revised:

Accepted:

Published:

Citation: Metzler Z., Kirschner N., Smith L., Cannady N., Sasaki M., Shy D., Caputo R., Kierans C., Bolotnikov A., Caligiure T. J., Carini G. A., Crosier A. W., Fried J., Ghosh P., Griffin S., Grove J. E., Hays E., Herrmann S., Kong E., Liceaga-Indart I., McEnery J., Mitchell J., Moiseev A. A., Parker L., Perkins J., Philips B., Schoenwald A. J., Sleator C., Thompson D. J., Valverde J., Wasti S., Woolf R., Wulf E., and Zajczyk A. Background Measurements and Simulations of the ComPair Balloon Flight. *Journal Not Specified* **2025**, *1*, 0. <https://doi.org/>

Copyright: © 2025 by the authors.

Submitted to *Journal Not Specified* for possible open access publication under the terms and conditions of the Creative Commons Attribution (CC BY) license (<https://creativecommons.org/licenses/by/4.0/>).

Abstract: ComPair, a prototype of the All-sky Medium Energy Gamma-ray Observatory (AMEGO), completed a short-duration high-altitude balloon campaign on August 27, 2023 from Fort Sumner, New Mexico, USA. The goal of the balloon flight was the demonstration of ComPair as both a Compton and Pair telescope in flight, rejection of the charged particle background, and measurement of the background γ -ray spectrum. This analysis compares measurements from the balloon flight with Monte Carlo simulations to benchmark the instrument. The comparison finds good agreement between the measurements and simulations and supports the conclusion that ComPair accomplished its goals for the balloon campaign. Additionally, two charged particle background rejection schemes are discussed: a soft ACD veto that records a higher charged particle event rate but with less risk of event loss, and a hard ACD veto that limits the charged particle event rate on board. There was little difference in the measured spectra from the soft and hard ACD veto schemes, indicating that the hard ACD veto could be used for future flights. The successes of ComPair's engineering flight will inform the development of the next generation of ComPair with upgraded detector technology and larger active area.

Keywords: Gamma Ray; ComPair; MeV γ -rays; Astroparticle; Instrumentation; AMEGO; Balloon

1. Introduction

The lack of sensitivity to astrophysical photons between ~ 100 keV and ~ 100 MeV relative to energies immediately above and below has earned this energy range the moniker

“MeV Gap.” There are multiple factors contributing to the MeV gap, including a) the need to discriminate between and image with both Compton scattering and pair production events, b) a minimum in the total photon interaction cross section, and c) a dominant charged particle background. The All-sky Medium Energy Gamma-ray Observatory (AMEGO) [1,2] is a NASA probe-class mission concept designed to overcome the challenges in order to fill the MeV gap. ComPair [3,4] is a prototype of AMEGO and consists of four detector subsystems – a 10-layer double-sided silicon strip detector Tracker [5–7], a Cadmium Zinc Telluride (CZT) Calorimeter [8], a thallium-doped Cesium Iodide (CsI) Calorimeter [9,10], and a plastic scintillator Anti-Coincidence Detector (ACD) [11]. These four detector systems work together to detect and characterize γ -rays that undergo Compton scattering or pair production. At low energies, the Tracker serves as the Compton scatterer, and at high energies, it acts as the pair conversion material. The CZT Calorimeter enhances the low energy sensitivity with good energy and position resolution, while the CsI Calorimeter enhances the high energy sensitivity with its stopping power. The ACD serves as an active shield to suppress the charged particle background, because it is generally insensitive to γ -rays but efficiently detects charged particles.

On August 27, 2023 ComPair conducted a short-duration high-altitude balloon flight from Fort Sumner, New Mexico, USA. The goals of this engineering flight was to demonstrate that the integrated system works as a Compton and Pair telescope in a space-like environment, to verify that the charged particle background rejection operates as intended, and to measure the background γ -ray spectrum. Successful completion of a short-duration flight is also a prerequisite for subsequent long-duration balloon flights.

Earlier papers have reported on the ComPair balloon flight. Kirschner et al. 2024 [7], Shy et al. 2024 [10], and Metzler et al. 2024 [11] each focus individually on the Tracker, CsI Calorimeter, and ACD, respectively. Smith et al. 2024 [12] highlights much of the pre-flight validation that is not considered here and also presents the measured flight spectra for each subsystem without applying the ACD veto or event reconstruction. In this analysis, we will demonstrate that the ComPair engineering flight achieved its goals by validating the measured ACD veto rate and event reconstruction with Monte Carlo simulations using MEGALib’s Cosima tool [13]. Section 2 describes the data analysis pipeline, simulations, and balloon flight in-general. Sections 3.1 and 3.2 compare the measured data to the background simulations, and Section 3.3 compares the effectiveness of a hard ACD veto, in which events are rejected during data collection, to a soft ACD veto, in which events are rejected only during data analysis, to inform their use on future ComPair balloon flights and AMEGO.

2. Materials and Methods

2.1. Event Selection

When a γ -ray or charged particle interacts in one of the detector subsystems, the subsystem will send a signal to the Trigger Module [14]. We call these signals ‘primitives.’ An event is defined by a unique event ID, which is created by the Trigger Module when primitives matching any of the following conditions are received from the detector subsystems.

1. Any 2 Tracker primitives
2. A single Tracker primitive and the CZT primitive
3. A single Tracker primitive and the CsI primitive
4. The CZT primitive and the CsI primitive

The Tracker produces one primitive for each side of each layer; and the CZT, CsI, and ACD each produce one primitive for the entire subsystem.

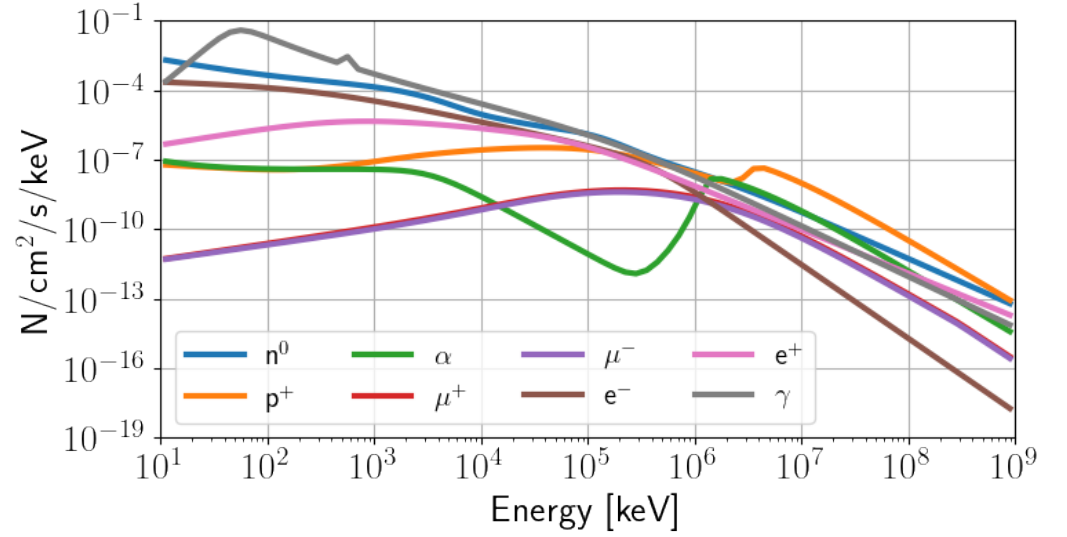


Figure 1. The angle-integrated particle background spectra for the ComPair balloon flight with 8 particle species as calculated with EXPACS [15]. EXPACS also provides azimuth-dependent spectra for each of these species, which were used to simulate the conditions during the flight with MEGALib's Cosima [13]. The settings used to produce this spectra are 34° latitude, -104° longitude, 40 km above sea level, 124 for the W value which is a measure of solar activity, and an ideal atmosphere surrounding environment.

The event ID's serve two purposes: event alignment and noise suppression. Each detector system has its own calibration pipeline, and the unique event ID is used to match simultaneous interactions in multiple detector systems. Requiring multiple primitives to define an event ID also suppresses noise triggers a single channel.

The Trigger Module also defines the two ACD veto modes - soft and hard. During soft ACD veto, the Trigger Module provides an event ID whether or not the ACD produces a primitive. During hard ACD veto, event IDs are provided only when the ACD does not produce a primitive.

2.2. Simulations and Event Reconstruction

To benchmark the measurements, we performed simulations of the high-altitude particle background using the EXcel-based Program for calculating Atmospheric Cosmic-ray Spectrum (EXPACS) [15]. EXPACS uses longitude, latitude, altitude, and solar activity to produce energy- and angular-dependent spectra for γ -rays, e^+ , e^- , p^+ , n^0 , μ^+ and μ^- , and α particles. Figure 1 shows the angle-integrated spectra for each particle species. A Monte Carlo simulation is performed with MEGALib's GEANT4-based Cosima tool [13,16]. The Cosima simulation records any interaction from γ -rays and particles in the active material of any subsystem, including the ACD.

The simulation includes tracking delayed emission due to nuclear activation by neutrons. The activation simulation is a three-step process. 1) An initial exposure tracks leptonic, photonic, and prompt emission due to nuclear excitations. This first phase also records the production of excited nuclei with longer decay times. 2) A build-up phase quickly extrapolates the production of the longer-lived nuclear excitations at the same rate as step 1). 3) The last phase propagates photons produced by the delayed emission of the longer-lived nuclear excitations. The times used for the ComPair balloon flight activation simulation were a 15-minute exposure, 1-hour activation build-up, and 15 minutes tracking the delayed nuclear de-excitations.

The simulated events are passed through the ComPair Detector Effects Engine (DEE), an internally developed python pipeline that applies instrumental effects and transforms

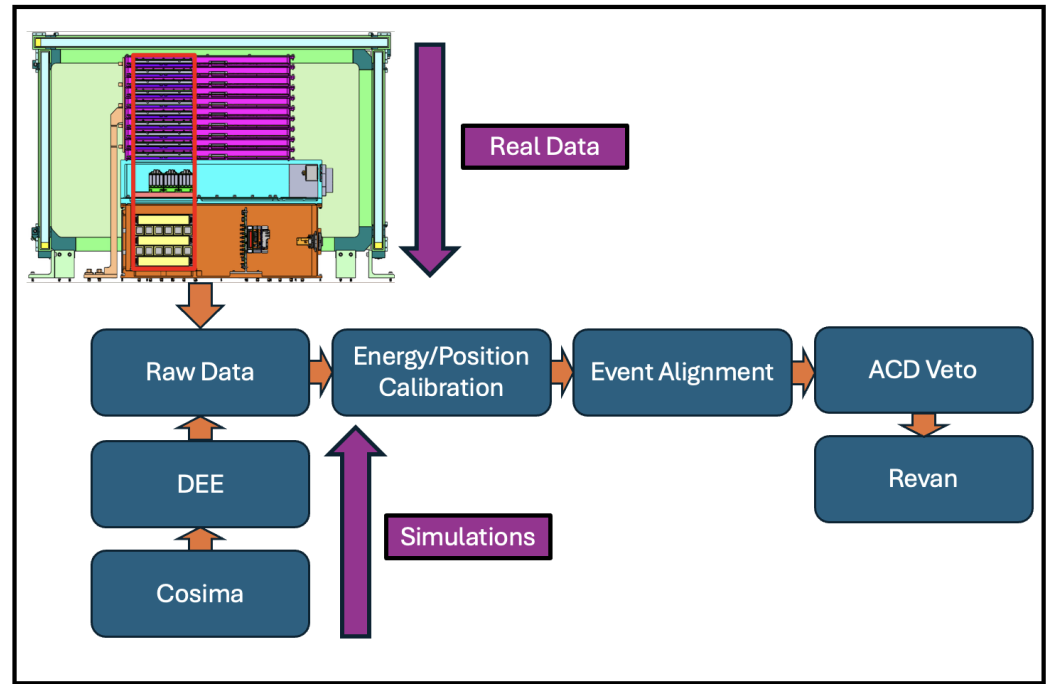


Figure 2. A schematic showing the steps performed on real and simulated data. Simulated interactions are produced with MEGALib’s Cosima [13] and transformed by the DEE to resemble raw data. Real raw data comes directly from the detector subsystems. Both real and simulated raw data undergoes energy and position calibrations, event alignment, an ACD veto, and event reconstruction offline. Event reconstruction classifies the remaining events into PH, CO, PA, and MU events.

the simulated interactions into a form resembling the raw output from the detectors. The instrumental effects include chance coincidence between multiple incident particles, detector dead time, trigger logic, thresholding, convolutions with noise pedestals, and converting to ADC values. Finally, the output of the DEE is passed through the same data analysis pipeline as the measured data.

Figure 2 shows a simple schematic of the steps for processing real and simulated data. The data analysis pipeline includes energy and position calibrations, event alignment between the detector subsystems, vetoing events that triggered the ACD.

Event reconstruction is performed with MEGALib’s Revan tool [13], which classifies the remaining events as photoabsorption (PH), Compton scattering (CO), pair production (PA), or muon tracks (MU), although particle MU events that pass the ACD veto are predominantly n^0 and p^+ at float altitude (see Table 2). Figure 3 shows examples of CO, PA, and MU events from real flight data. Among multi-hit events, Revan will first search for PA events (center panel of Fig. 3), which are fit by two tracks that meet at a vertex. Reconstructed PA events point directly to the γ -ray source. If the event is not a PA event, Revan will look for MU events, which are defined by a single track. An example vetoed MU event is shown in the left panel of Fig. 3. MU events are not used for imaging. Finally, Revan will attempt to find a valid Compton scattering sequence for any non-PA and non-MU events. If a valid sequence is found, the event is classified as a CO event (right panel of Fig. 3). Reconstructed CO events project to a ring in the sky that overlaps with the γ -ray source. Any event without a valid Compton scattering sequence is rejected.

2.3. Balloon Flight Overview

ComPair’s balloon flight from Ft Sumner, NM, USA in 2023 was 6 hours and 17 minutes long, of which 3 hours and 13 minutes were over 40 km above sea level. Figure 4 shows the altitude and event rate as a function of time. Data were collected in 30-minute

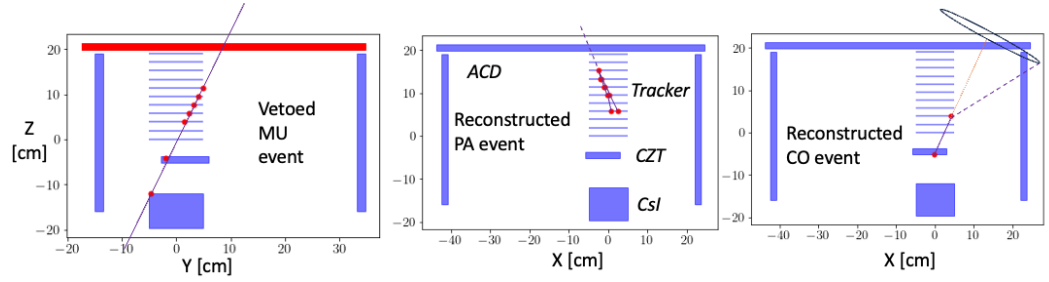


Figure 3. Examples of MU, PA, and CO events from the balloon flight, where the triggered hits are shown as red dots. A MU event triggers the top ACD panel, consists of a single track, and is not used for imaging. A PA event consists of two tracks that intersect at a vertex, and can be pointed back to its source along a single direction. This PA event seems to stop in the Tracker, because the tracks exit the side of the Tracker before reaching the CZT Calorimeter. Any events with multiple hits that are not MU or PA are reconstructed as CO events if a valid Compton scattering sequence can be found. Events with a valid Compton scattering sequence can point back to a ring in the sky where the photon originated, events without a valid sequence are rejected.

segments during the flight, marked by the vertical dashed lines. The green bands represent the soft ACD veto, and the yellow band covers a test of the hard ACD veto. The hard ACD veto substantially reduces the event rate but increases the risk of event loss if the ACD malfunctions. The green bands total 90 minutes, and the yellow band covers 11 minutes.

The DC-DC converter for the main power distribution unit's temperature became too hot to safely operate during the two gray segments, so we turned ComPair off to cool to an appropriate temperature. Unfortunately, the Tracker data was not recoverable for the two red segments, so only the times in the green bands of Figure 4 are used for the analysis of the soft veto mode at float altitude. The two gray segments span 12 and 10 minutes, and the red segments span 26 and 19 minutes.

3. Results and Discussion

3.1. Soft ACD Veto Efficiency

A key benchmark for ComPair's balloon flight is the effectiveness of the ACD to reject charged particles, while passing (not vetoing) γ -rays. Table 1 shows event rates before and after applying the soft ACD veto, wherein events are rejected after the event alignment step of Figure 2 if there is an interaction in the ACD. The first two rows show the overall measured and simulated event rates, respectively. Rows 3–12 show the event rates for each simulated particle species, where activation is defined as the delayed emission due to nuclear de-excitations and coincidence is when any 2 simulated particles interact within 20 ns. The real measured data rate is $\approx 20\%$ greater than the simulated total. This could be due to the simulated geometry not accounting for all of the passive material aboard the flight gondola or other unknown effects not included in the DEE. Before applying the ACD veto, the dominant particle types are protons and alpha particles, while γ -rays are third at just under 15% of the simulated events. After applying the veto, γ -rays make up just over 68% of the simulated events and now dominate over the charged particle background, validating the efficiency of the ACD.

Figure 5 shows the same information as Table 1 as the percentage of each particle type that is vetoed by the ACD. Over 99% of protons, muons, and alpha particles are rejected by the ACD, while most γ -rays and events due to activation pass. Activation is particularly challenging to veto, because the delayed de-excitation is not coincident with the incident particle. Therefore, the primary particle that causes the excitation could be vetoed, but the delayed emission likely will not.

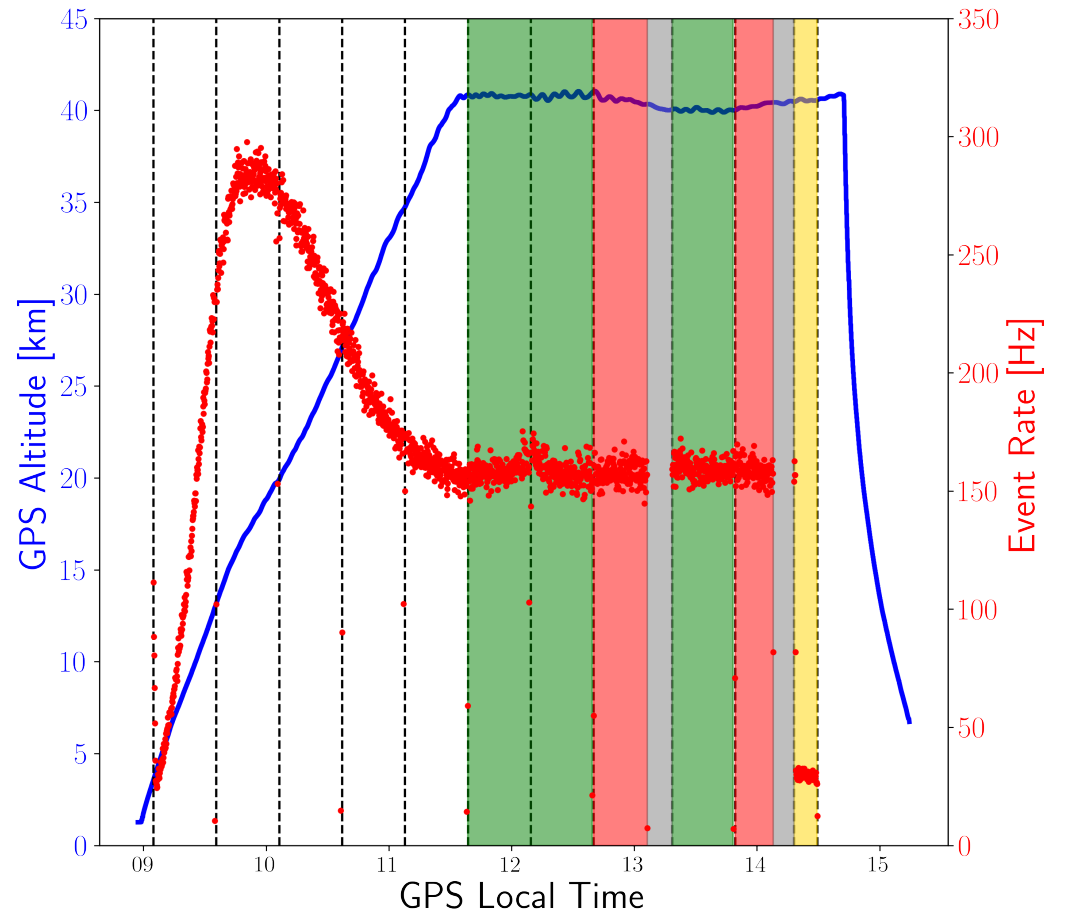


Figure 4. Blue: the altitude throughout the balloon flight. Red: the number of unique event IDs produced per second during the flight. The times given are the local date and time in New Mexico, USA. The green bands indicate the times used to analyze the soft ACD veto, and the yellow band covers the hard ACD veto. The gaps in the data are due to overheating of the main power distribution unit, which had to be turned off and allowed to cool before restarting operations.

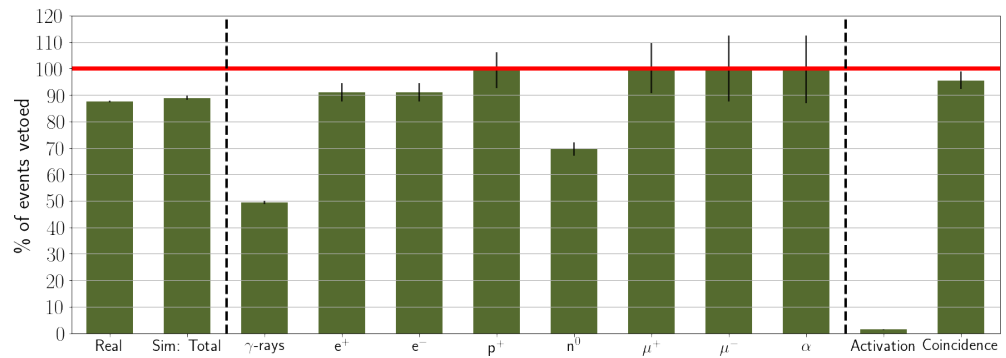


Figure 5. A comparison of the veto rates between the real and simulated data. The red line at 100% corresponds to all events being rejected. The first column shows the measured data, the second column shows the total of the simulated data, columns 3–10 show the simulation divided by particle type. Column 11 represents the simulated events due to activation within the instrument or passive material. Column 12 is for events where two simulated particles interacted with the detector within 20 μ s, and so were assigned to a single event.

Figure 5 shows that $\sim 50\%$ of γ -rays are vetoed by the ACD, and it is important to understand the cause. Figure 6 shows the total spectrum of incident simulated γ -ray energies that satisfy ComPair's trigger conditions in blue as well as the spectra for passed and vetoed γ -rays in orange and green, respectively. There is a crossover between the passed and vetoed γ -ray spectrum around 100 MeV, above which a majority of the incident γ -rays are vetoed by the ACD. A larger instrument, like AMEGO, would model the showers produced by high energy γ -rays and override the ACD veto for these types of events, but this is beyond the scope for ComPair.

Table 1. A comparison of the event rates before and after the soft ACD veto is applied. The first row shows the measured data, the second row shows the total of the simulated data, rows 3–10 show the simulation divided by particle type. Row 11 is for simulated activation, nuclear excitations caused by high energy protons, neutrons and alpha particles. Row 12 is for events where two simulated particles interacted with the detector within 20 μ s, and so were assigned to a single event.

Particle Selection	Initial Rate Events/s	Post-veto Rate Events/s
–		
Measured Total	145.6	18.2
Simulated Total	121.2	13.4
γ-rays	18.1	9.2
e ⁺	9.4	0.8
e ⁻	8.7	0.8
p ⁺	36.4	0.2
n ⁰	3.8	1.2
μ ⁺	0.1	0.0
μ ⁻	0.1	0.0
α	21.9	0.1
Activation	0.2	0.2
Coincidence	22.4	1.0

3.2. Event Reconstruction & Spectra

The events that pass the ACD veto stage are reconstructed with Revan and sorted into PH, CO, MU, and PA events. Some events are outright rejected for having no valid Compton scattering sequence, among other reasons. Approximately half of the events pass reconstruction. Table 2 shows the event rates for the measured real data and simulations

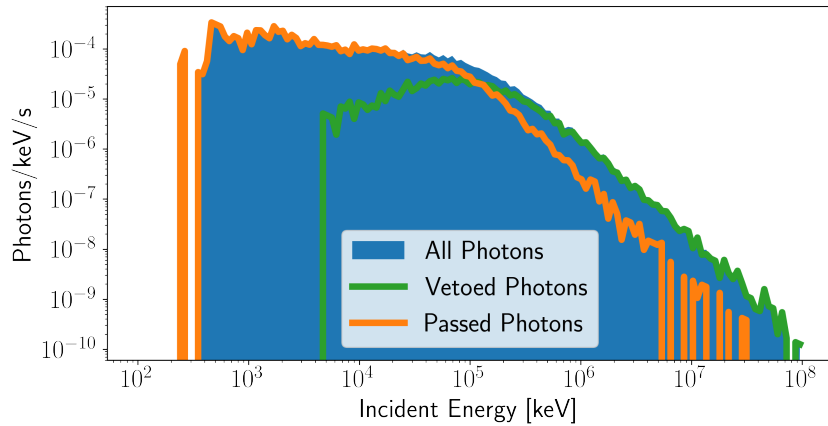


Figure 6. A spectrum of the incident energies of simulated photons that satisfied ComPair’s trigger conditions. The total spectrum is shown in blue, while the orange and green lines show the spectra for passed (not vetoed) and vetoed photons, respectively. This shows that the 50% of γ -rays that are vetoed are high energy photons, which likely produce a shower that triggers the ACD.

divided into the reconstructed event type. The rows are similar to Table 1, except that the muon rows have been removed, because 100% of the muons were vetoed in the simulation. The reconstructed event rates underscore that the final product of our data analysis and reconstruction pipeline is predominantly γ -rays as 67% of the simulated events at this stage are photons, and 82% of the reconstructed PA events are photons. The real measured data has an 15% higher event rate than the simulation, and about twice the MU rate as the simulation. This difference is likely due to discrepancies between the simulation mass model and the instrument.

The reconstructed event rates in Table 2 also highlight a common issue facing MeV telescopes: the charged particle background is misidentified as γ -ray interactions. In Table 2, CO and PA should be purely γ -ray interactions, but all non- γ -ray event types also appear in the simulated CO data, and e^- and e^+ appear in the simulated PA data. For Revan, it searches first for PH events, because they only have a single interaction. Then it will search for two tracks and a vertex for PA events, followed by a search for a single track for a MU event. Finally, it will search for a valid Compton scattering sequence and call those CO events. Events without a valid Compton scattering sequence are rejected. This means that charged particles can also end up in the CO category, or that γ -rays can be reconstructed as MU events if a tracked Compton electron is misidentified or one of the pair-produced particles escapes. Nevertheless, improvements to the reconstruction methodology is beyond the scope of this work, and γ -rays still dominate over the charged particle background after the ACD veto and reconstruction.

Figure 7 shows the spectra of the total energy deposited in the detectors by event for both the real and simulated data, separated by reconstructed event type. The real data is shown as points with 1σ error bars spanning the histogram bin widths, and the solid lines are the simulated data.

The real and simulated spectra generally agree, except there seems to be a discrepancy regarding the threshold, which causes the simulation to underestimate the real data by 0.5 Events/s below 200 keV, and that the real data has a peak in the MU event spectrum near 500 keV that does not appear in the simulation.

Also near 500 keV, the simulated Compton spectrum overestimates the measurement. This could be due to incorrectly reconstructing of Compton scattered electrons as MU tracks when the Compton scattered photon escapes in the real data. In this case, the DEE may not fully account for some inefficiencies in the detectors that result in losing the Compton

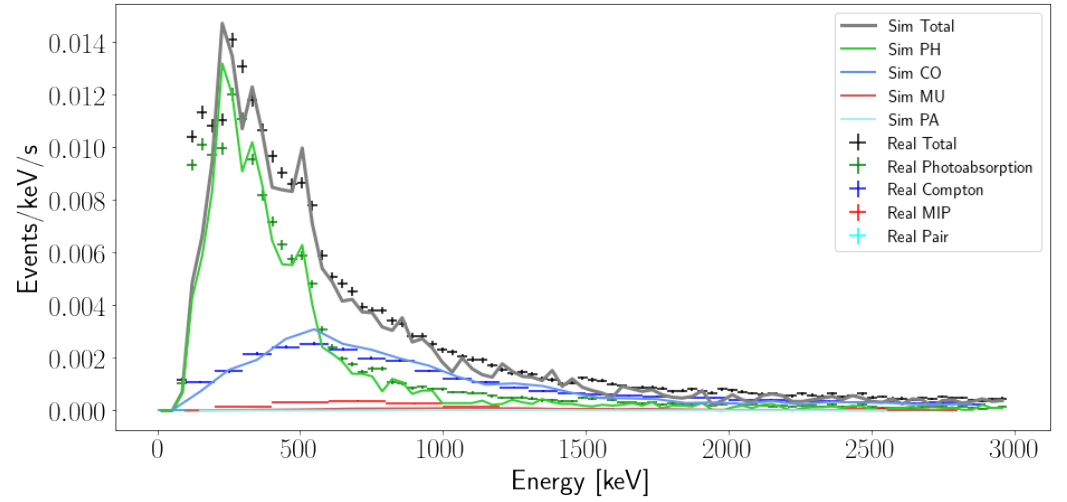


Figure 7. Spectra of the measured energy deposit per event after event reconstruction for the real and simulated data. The points are the real data with 1σ uncertainty within the histogram's bins, and the lines are the simulations.

scattered photons. There is also a difference in the prominence of the 511 keV line, which appears sharper in the simulated data than in the measurement. This is likely due to ComPair's energy calibration not accounting for thermal effects, the temperature change during the flight shifts the gain and energy thresholds of the detectors and smear the energy response. The DEE also does not account for the changing temperature, and therefore leaves a sharp 511 keV line. Despite these two minor discrepancies, the simulations and the real data are well matched during the balloon flight.

Table 2. A comparison of the reconstruction rates between the measured real data (first row) and the simulated data. The second row presents the total simulated data, while rows 3–9 show the simulations by particle type. Row 10 shows events where 2 particles interacted with ComPair within $20 \mu\text{s}$ during the simulation. These rates highlight both the effectiveness of the charge particle rejection, that reconstruction maintains γ -rays dominating over charged particles in our dataset, and that the reconstructed charged particle interactions are often reconstructed as CO events, while γ -rays are sometimes classified as MU events.

Particle Selection	Recon. Rate	PH Rate	CO Rate	MU Rate	PA Rate
–	Events/s	Events/s	Events/s	Events/s	Events/s
Measured Total	10.3	5.6	4.3	0.4	0.02
Simulated Total	8.9	4.7	4.1	0.2	0.02
γ -rays	6.0	3.2	2.7	0.09	0.02
e^+	0.5	0.2	0.3	0.01	0.001
e^-	0.4	0.2	0.3	0.01	0.002
p^+	0.1	0.05	0.06	0.03	0
n^0	1.0	0.5	0.4	0.03	0
α	0.04	0.02	0.02	0.001	0
Activation	0.2	0.1	0.03	0	0
Coincidence	0.7	0.4	0.3	0.01	0.001

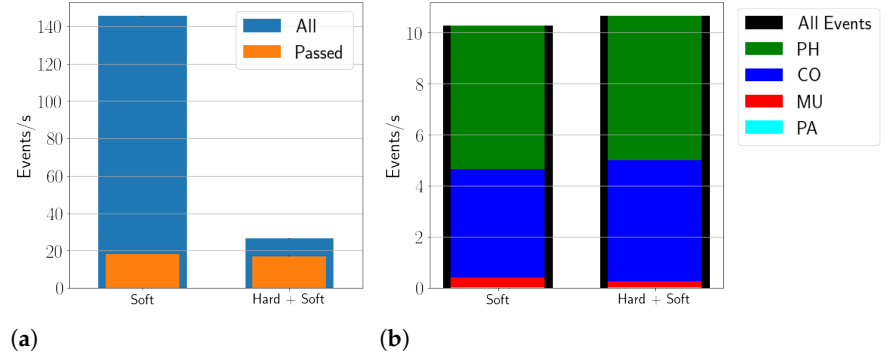


Figure 8. (a) A comparison of the pre- and post-ACD soft vetos for the datasets collected during the green and yellow bands from Figure 4. The first column represents the green band and the second column is the yellow band. The blue and orange bars show the event rates before and after applying a soft ACD veto, respectively. A concern before this test was that the hard ACD veto might reduce the event rate to below that of the soft veto if Trigger Module timing was off. This result gives confidence that the hard ACD veto could be used in future iterations of ComPair and AMEGO. **(b)** A comparison of the pre- and post-ACD vetos for the datasets collected during the green and yellow bands from Figure 4. The first column represents the green bands and the second column is the yellow band. The bars are divided based on reconstructed event type, and show little difference between using soft veto only or hard veto.

3.3. Testing the ACD Hard Veto

Looking ahead to AMEGO, possible future challenges are high event rates that severely limit the live time of the instrument and necessitate down linking events due to background particles. With this in mind, we used the final 11 minutes of the balloon flight to test a hard ACD veto (the yellow band of Figure 4), where the Trigger Module does not provide an event ID if it receives a primitive from the ACD during data collection. Using a hard veto can be risky, due to the possibility that no event IDs would be produced for event alignment between the other three detectors if the Trigger Module timing is misaligned, hence losing some data. The goal of this test is to determine that the hard ACD veto did not result in a change in the measured spectrum.

Comparing the event rates using the hard veto to the soft veto from Section 3.1, we found that the hard veto was not 100% efficient, as there were still events with event IDs and energy deposited in the ACD. This necessitates applying an additional soft ACD veto following the hard ACD veto. This is shown in Figure 8(a), where the blue and orange bars represent the event rates before and after the “ACD Veto” step of Figure 2, respectively, and the “Soft” and “Hard + Soft” columns represent the green and yellow bands from Figure 4, respectively. The hard ACD veto was not 100% efficient, because the blue bar of the “Hard + Soft” column is higher than either orange bar. The hard ACD veto being less efficient could have been due to an inefficiency in the ACD sending a primitive to the Trigger Module. This trigger primitive inefficiency has also been observed with other detector systems.

Figure 8(b) shows the event rates for the same categories after event reconstruction with Revan. At this stage, the “Hard + Soft” category has retained a higher event rate than the soft-only, which suggests that the event rate variations between the two vetoing schemes are due to statistical fluctuations and not any malfunction of the ACD hard veto. The spectra in Figure 9 also supports the conclusion that the hard ACD veto did not affect the measured γ -ray spectrum, as the soft-veto only and hard-then-soft-veto spectra follow one another closely. For these reasons, the hard veto was validated to be used for future iterations of ComPair or AMEGO with lower down link requirements.

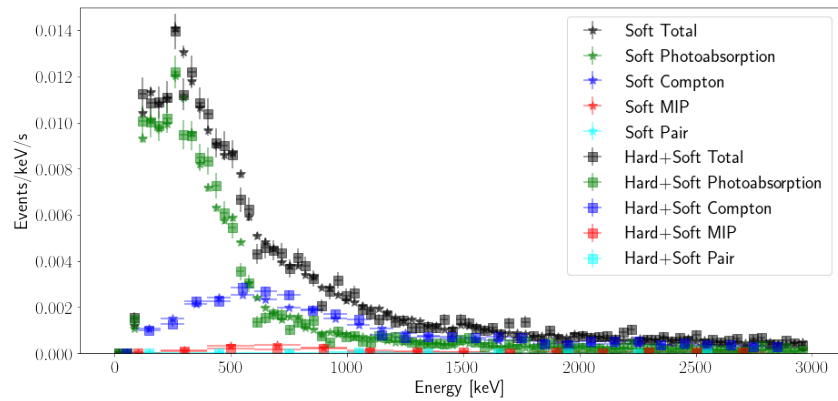


Figure 9. Spectra separated by reconstructed event type for events with soft veto only (solid lines) and a hard veto followed by soft veto (dashed lines). The veto scheme did not compromise the measured spectra, validating the hardware implementation

4. Conclusions

The ComPair high-altitude balloon flight successfully measured the γ -ray background at a float altitude of ≈ 40 km above sea level. The ACD veto and event reconstruction were validated by Monte Carlo simulations of the particle background at float altitudes by comparing event rates and measured spectra. This engineering flight demonstrated effective rejection of the charged particle background with the ACD, and showed that a hard ACD veto could be used to limit data down link without altering the measured γ -ray spectrum. Looking forward, the success of ComPair's 2023 balloon flight sets the stage for ComPair-2 [17] with ~ 16 times larger active area and raising the technology readiness levels of several key technologies for AMEGO-X [18,19], a medium explorer-class concept similar to AMEGO.

Author Contributions: Conceptualization, D.T., B.P., J.McE., E.G., E.H., A.M., J.P., and E.W.; methodology, Z.M., N.C., R.C., C.K., N.K., L.S., M.S., D.S., R.W., A.M.; software, Z.M., S.W., A.Z., N.K., N.C., L.S., L.P., M.S., D.S., S.G., and P.G.; validation, Z.M.; formal analysis, Z.M., L.S., N.K., and D.S.; investigation, Z.M., N.C., R.C., C.K., N.K., L.S., L.P., A.S., R.W., D.S., A.C., T.C., J.V., E.K., S.G., I.L., J.M., C.S., and A.M.; resources, J.F., A.B., G.C., and S.H.; data curation, Z.M., L.S., N.K., and D.S.; writing—original draft preparation, Z.M.; writing—review and editing, Z.M., N.K., L.S., N.C., R.C., C.K., M.S., D.S., R.W., and A.M.; visualization, Z.M. and N.K.; supervision, R.C., C.K., R.W., and A.M.; project administration, R.C. and C.K.; funding acquisition, J.McE., E.G., C.K., and R.W. All authors have read and agreed to the published version of the manuscript.

Funding: This work is supported under NASA Astrophysics Research and Analysis (APRA) grants NNH14ZDA001NAPRA, NNH15ZDA001N-APRA, NNH18ZDA001N-APRA, NNH21ZDA001N-APRA.

Data Availability Statement: The raw data supporting the conclusions of this article will be made available by the authors on request.

Acknowledgments: The material is based upon work supported by NASA under award number 80GSFC24M0006. Daniel Shy is supported by the U.S. Naval Research Laboratory's Jerome and Isabella Karle Distinguished Scholar Fellowship Program. A. W. Crosier and T. Caligiure would like to acknowledge the Office of Naval Research NREIP Program.

Conflicts of Interest: The authors declare no conflicts of interest. The funders had no role in the design of the study; in the collection, analysis, or interpretation of the data; in the writing of the manuscript; or in the decision to publish the results.

Abbreviations

The following abbreviations are used in this manuscript:

ACD	Anti-Coincidence Detector
AMEGO	All-sky Medium Energy Gamma-ray Observatory
AMEGO-X	All-sky Medium Energy Gamma-ray Observatory eXplorer
CO	Compton scattering
CsI	Cesium Iodide
CZT	Cadmium Zinc Telluride
DEE	Detector Effects Engine
EXPACS	EXcel-based Program for calculating Atmospheric Cosmic-ray Spectrum
GEANT4	GEometry ANd Tracking 4
MU	Muon track
PA	Pair production
PH	Photoabsorption

References

1. McEnery, J.; Barrio, J.A.; Agudo, I.; Ajello, M.; Álvarez, J.M.; Ansoldi, S.; Anton, S.; Auricchio, N.; Stephen, J.B.; Baldini, L.; et al. All-sky Medium Energy Gamma-ray Observatory: Exploring the Extreme Multimessenger Universe, 2019, [[arXiv:astro-ph.IM/1907.07558](https://arxiv.org/abs/1907.07558)].
2. Kierans, C.A. AMEGO: exploring the extreme multi-messenger universe. In Proceedings of the Space Telescopes and Instrumentation 2020: Ultraviolet to Gamma Ray; den Herder, J.W.A.; Nakazawa, K.; Nikzad, S., Eds. SPIE, 12 2020. <https://doi.org/10.1117/12.2562352>.
3. Shy, D.; Kierans, C.A.; Cannady, N.; Caputo, R.; Griffin, S.; Grove, E.; Hays, E.; Kong, E.; Kirschner, N.; Liceaga-Indart, I.; et al. Development of the ComPair gamma-ray telescope prototype. In Proceedings of the Space Telescopes and Instrumentation 2022: Ultraviolet to Gamma Ray; den Herder, J.W.A.; Nakazawa, K.; Nikzad, S., Eds. SPIE, 8 2022, p. 92. <https://doi.org/10.1117/12.2628811>.
4. Valverde, J.; Kirschner, N.; Metzler, Z.; Smith, L.D.; Cannady, N.W.; Caputo, R.; Kierans, C.; Liceaga-Indart, I.; Moiseev, A.; Parker, L.; et al. The Compton Pair telescope: A prototype for a next-generation MeV gamma-ray observatory. In Proceedings of the Proceedings of 38th International Cosmic Ray Conference — PoS(ICRC2023). Sissa Medialab, 8 2023, ICRC2023, p. 857. <https://doi.org/10.22323/1.444.0857>.
5. Griffin, S.; the AMEGO Team. Development of a Silicon Tracker for the All-sky Medium Energy Gamma-ray Observatory Prototype, 2019, [[arXiv:astro-ph.IM/1902.09380](https://arxiv.org/abs/1902.09380)].
6. Griffin, S.; Kierans, C.; Parker, L.; Schoenwald, A.; Shawhan, P.; Caputo, R.; McEnery, J.; Perkins, J. Current status of the ComPair silicon tracker. In Proceedings of the Space Telescopes and Instrumentation 2020: Ultraviolet to Gamma Ray; den Herder, J.W.A.; Nikzad, S.; Nakazawa, K., Eds. International Society for Optics and Photonics, SPIE, 2020, Vol. 11444, p. 1144434. <https://doi.org/10.1117/12.2561909>.
7. Kirschner, N.; Kierans, C.; Wasti, S.; Schoenwald, A.J.; Caputo, R.; Griffin, S.; Liceaga-Indart, I.; Parker, L.; Perkins, J.S.; Zajczyk, A. The Double-Sided Silicon Strip Detector Tracker onboard the ComPair Balloon Flight, 2024, [[arXiv:astro-ph.IM/2407.18737](https://arxiv.org/abs/2407.18737)].
8. Hays, E.A.; Bolotnikov, A.; Kierans, C.; Moiseev, A.; Thompson, D. Modular Position-sensitive High-resolution Calorimeter for Use in Space Gamma-ray Instruments Based on Virtual Frisch-grid CdZnTe Detectors. *PoS* **2019**, *ICRC2019*, 584. <https://doi.org/10.22323/1.358.0584>.
9. Woolf, R.S.; Grove, J.E.; Philips, B.F.; Wulf, E.A. Development of a CsI:Tl calorimeter subsystem for the All-Sky Medium-Energy Gamma-Ray Observatory (AMEGO), 2019, [[arXiv:physics.ins-det/1901.05828](https://arxiv.org/abs/1901.05828)].
10. Shy, D.; Woolf, R.S.; Sleator, C.; Philips, B.; Grove, J.E.; Wulf, E.A.; Johnson-Rambert, M.; Davis, M.; Kong, E.; Caligiure, T.; et al. Results from the CsI Calorimeter onboard the 2023 ComPair Balloon Flight, 2024, [[arXiv:astro-ph.IM/2405.06839](https://arxiv.org/abs/2405.06839)].
11. Metzler, Z.; Cannady, N.; Shy, D.; Caputo, R.; Kierans, C.; Woolf, R. The Anti-Coincidence Detector Subsystem for ComPair, 2024, [[arXiv:astro-ph.IM/2405.15974](https://arxiv.org/abs/2405.15974)].
12. Smith, L.D.; Cannady, N.; Caputo, R.; Kierans, C.; Kirschner, N.; Liceaga-Indart, I.; McEnery, J.; Metzler, Z.; Moiseev, A.A.; Parker, L.; et al. The 2023 balloon flight of the ComPair instrument. In Proceedings of the Space Telescopes and Instrumentation 2024: Ultraviolet to Gamma Ray; den Herder, J.W.A.; Nakazawa, K.; Nikzad, S., Eds. SPIE, 8 2024, p. 303. <https://doi.org/10.1117/12.3020463>.
13. Zoglauer, A.; et al. MEGALib The Medium Energy Gamma-ray Astronomy Library. *New Astr. News* **2006**, *50*, 629–632. <https://doi.org/10.1016/j.newar.2006.06.049>.

14. Sasaki, M. Trigger system for the ComPair instrument. In Proceedings of the Space Telescopes and Instrumentation 2020: Ultraviolet to Gamma Ray; den Herder, J.W.A.; Nikzad, S.; Nakazawa, K., Eds. International Society for Optics and Photonics, SPIE, 2020, Vol. 11444, p. 114446A. <https://doi.org/10.1117/12.2561658>.
15. Sato, T. Analytical model for estimating the Zenith Angle Dependence of terrestrial cosmic ray fluxes. *PLOS ONE* **2016**, *11*. <https://doi.org/10.1371/journal.pone.0160390>.
16. Agostinelli, S.; Allison, J.; Amako, K.; Apostolakis, J.; Araujo, H.; Arce, P.; Asai, M.; Axen, D.; Banerjee, S.; Barrand, G.; et al. Geant4—a simulation toolkit. *Nuclear Instruments and Methods in Physics Research Section A: Accelerators, Spectrometers, Detectors and Associated Equipment* **2003**, *506*, 250–303. [https://doi.org/10.1016/S0168-9002\(03\)01368-8](https://doi.org/10.1016/S0168-9002(03)01368-8).
17. Caputo, R.; Kierans, C.; Cannady, N.; Falcone, A.D.; Fukazawa, Y.; Jadhav, M.; Kerr, M.; Kirschner, N.; Kumar, K.; Laviro, A.; et al. ComPair-2: a next-generation medium-energy gamma-ray telescope prototype. In Proceedings of the Space Telescopes and Instrumentation 2024: Ultraviolet to Gamma Ray; den Herder, J.W.A.; Nakazawa, K.; Nikzad, S., Eds. SPIE, 8 2024, p. 94. <https://doi.org/10.1117/12.3017619>.
18. Fleischhack, H. AMEGO-X: MeV gamma-ray Astronomy in the Multimessenger Era, 2021, [[arXiv:astro-ph.IM/2108.02860](https://arxiv.org/abs/2108.02860)].
19. Caputo, R.; Ajello, M.; Kierans, C.A.; Perkins, J.S.; Racusin, J.L.; Baldini, L.; Baring, M.G.; Bissaldi, E.; Burns, E.; Cannady, N.; et al. All-sky Medium Energy Gamma-ray Observatory eXplorer mission concept. *Journal of Astronomical Telescopes, Instruments, and Systems* **2022**, *8*. <https://doi.org/10.1117/1.jatis.8.4.044003>.

Disclaimer/Publisher’s Note: The statements, opinions and data contained in all publications are solely those of the individual author(s) and contributor(s) and not of MDPI and/or the editor(s). MDPI and/or the editor(s) disclaim responsibility for any injury to people or property resulting from any ideas, methods, instructions or products referred to in the content.